ACS APPLIED MATERIALS & INTERFACES

Research Article

www.acsami.org

Non-Faradaic Electrical Impedimetric Investigation of the Interfacial Effects of Neuronal Cell Growth and Differentiation on Silicon Nanowire Transistors

Shu-Ping Lin,*[,†,§] Lester U. Vinzons,[†,§] Yu-Shan Kang,[†] and Tung-Yen Lai[‡]

[†]Graduate Institute of Biomedical Engineering, National Chung Hsing University, Taichung 40227, Taiwan, R.O.C.

[‡]National Nano Device Laboratories, Hsinchu 30078, Taiwan, R.O.C.

Supporting Information

ABSTRACT: Silicon nanowire field-effect transistor (SiNW FET) devices have been interfaced with cells; however, their application for noninvasive, real-time monitoring of interfacial effects during cell growth and differentiation on SiNW has not been fully explored. Here, we cultured rat adrenal pheochromocytoma (PC12) cells, a type of neural progenitor cell, directly on SiNW FET devices to monitor cell adhesion during growth and morphological changes during neuronal differentiation for a period of 5−7 d. Monitoring was performed by measuring the non-Faradaic electrical impedance of the cell−SiNW FET system using a precision LCR meter. Our SiNW FET devices exhibited changes in impedance parameters during cell growth and differentiation because of the negatively charged cell membrane, seal resistance, and membrane capacitance at the cell/SiNW interface. It was observed that during both PC12 cell growth and neuronal differentiation, the impedance magnitude increased and the phase shifted to more negative values. However, impedance changes during cell growth already plateaued 3 d after seeding, while impedance changes continued until the last observation day during differentiation. Our results also indicate that the frequency shift to above 40 kHz after growth factor induction resulted from a larger coverage of cell membrane on the SiNWs due to distinctive morphological changes according to vinculin staining. Encapsulation of PC12 cells in a hydrogel scaffold resulted in a lack of trend in impedance parameters and confirmed that impedance changes were due to the cells. Moreover, cytolysis of the differentiated PC12 cells led to significant changes in impedance parameters. Equivalent electrical circuits were used to analyze the changes in impedance values during cell growth and differentiation. The technique employed in this study can provide a platform for performing investigations of growth-factor-induced progenitor cell differentiation.

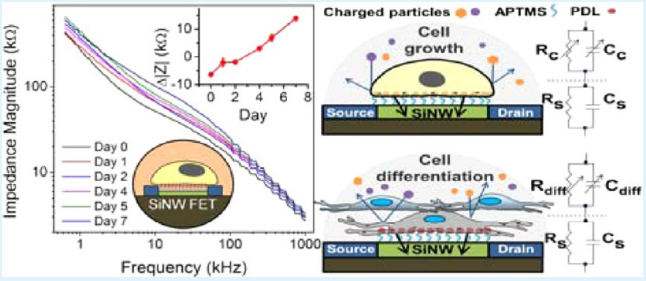

KEYWORDS: *silicon nanowire, field-effect transistor, non-Faradaic electrical impedance, cell growth, cell differentiation*

1. INTRODUCTION

Cell-based biosensors have been extensively studied in the past decades because of their potential application in various fields such as drug discovery,[1,2] environmental screening,[3−6] and food safety.[3,4,7] These biosensors, which usually employ optical or electrical detection schemes, exploit the native recognition elements of cells to detect a broad range of known and unknown agents and to obtain functional information on the effect of these agents on a living system. Electrical biosensors have been preferred over optical readout-based sensors because of their high sensitivity and selectivity, ability to be used in turbid solutions, amenability to miniaturization, real-time response to external stimulation, and ability to convey the intracellular condition.[8] Non-Faradaic electrical impedance spectroscopy (EIS) has been typically used to characterize the interfacial properties of biomaterials or cells associated with conductive or semiconductive devices.[9−14] Such interfacial information on the electrical characteristics external to the sensing device is only limited to the nature of charged species (i.e., either positive or negative) and their concentration near the sensing surface instead of induced changes in Faradaic electrochemical reactions. Therefore, the measured signals of non-Faradaic EIS are attributed to the insulating effects of cell membranes of cells that grow on or attach to the sensing surface.[10,14] In addition, the changes in cell number and isolation of charged particles from the sensing surfaces have a great impact on impedance parameters, such as resistance and capacitance.[9,11,12,14]

At present, cell-based biosensors are applied in electrophysiological recordings on electrogenic cells based on intracellular patch-clamp techniques[15] and extracellular multielectrode arrays (MEAs).[9,14,16] Patch-clamp-derived techniques provide better signal-to-noise ratios; however, they are invasive, require trained personnel or specialized laboratory equipment,

Received: March 2, 2015
Accepted: April 22, 2015
Published: April 22, 2015

DOI: 10.1021/acsami.5b01878
ACS Appl. Mater. Interfaces 2015, 7, 9866−9878

have low throughput, and may not allow long-term monitoring.[17−22] On the other hand, noninvasive extracellular MEA systems enable electrophysiological recordings on large populations of cells for long-term observation. Nevertheless, the relatively high impedance of the microscale electrodes attenuates cellular signals, and the recorded synergistic signals are difficult to be distinguished into specific signals from individual cells.[9,17,19,23]

In recent years, breakthroughs in nanotechnology have given rise to new materials and devices that have enabled revolutionary ways of probing cellular activities.[20−22,24] Among these nanoscale devices, silicon nanowire field-effect transistor (SiNW FET) devices have been widely studied and applied with the aim of developing cell-based biosensors owing to their high selectivity and sensitivity, real-time response, and label-free detection capabilities.[21,22,24−27] The high sensitivity of SiNW FETs is due to the combined effect of the high surface-to-volume ratio of the SiNW channel and FET amplification: small changes in charge concentration in the immediate environment greatly affect the conductivity of the channel, while FET amplification in saturation mode enhances device performance in weak-signal applications.[28] Solutions from chemically or electrically stimulated cells have been collected and dispensed onto receptor-functionalized SiNW FET devices for the indirect detection of specific biomolecules.[25,29,30] Electrogenic cells have also been successfully interfaced with patch-clamp-based SiNW FETs to monitor action potential changes caused by electrical or chemical stimulation.[18,24,26,31−34] These studies have shown that SiNW FET devices can detect biomolecules with high selectivity and sensitivity, as well as detect action potential signals from individual cells with high temporal and spatial resolution. However, noninvasive cellular monitoring using SiNW FET devices is necessary because patch-clamp-based SiNW FET devices compromise the integrity of cells and drastically decrease the duration of stable recording.[17]

To provide a platform for long-term investigations of growth-factor-induced progenitor cell differentiation, cell/SiNW interfacing was created and used in this study to examine time-course changes in cell conditions. The use of SiNW FETs for the noninvasive time-course monitoring of cell adhesion and morphological changes of rat adrenal pheochromocytoma (PC12) cells, a type of neural progenitor cell, during growth and neuronal differentiation, respectively, was demonstrated. We monitored the changes in the electrical properties of the cell−SiNW FET system using non-Faradaic EIS, an established technique for biomolecular detection and cell characterization.[9−12,14] We hypothesized that the high sensitivity of the SiNW FET to minute changes in the surrounding charges can lead to measurable changes in the impedance magnitude and impedance phase owing to the coupling of cells with charged cell membranes onto the nanowire and/or the screening of charged species in the surrounding solution by the cells.

2. EXPERIMENTAL PROCEDURES

2.1. Fabrication of SiNW FET Devices and Culture Chambers. Single-SiNW *n*-type FET devices were used for the observation of PC12 cell adhesion, while multi-SiNW *n*-type FET devices were used for the observation of PC12 neuronal differentiation. Both types of SiNW FET devices were fabricated in National Nano Device Laboratories (Hsinchu, Taiwan) using a "top-down" process similar to that used in our previous study.[35] The general procedure comprises the following steps: Standard 6 in. p-type Si wafers were coated with insulating layers, composed of SiO_2 (100 nm) and Si_3N_4 (30 nm), and a layer of polysilicon (poly-Si; 100 nm) using CVD. The poly-Si layer was annealed at 900 °C for 24 h to enhance crystallization. To form the SiNW and source and drain terminals of the devices, photoresist (PR) was patterned over the poly-Si layer using an i-line stepper. The poly-Si was etched using an inductively coupled plasma (ICP) etcher (TCP 9400, Lam Research) with a $HBr/Cl_2/O_2$ chemistry. The dimensions of the SiNWs were further reduced by first performing dry oxidation of the poly-Si to form 20 nm thick SiO_2 and then by etching the SiO_2 using hydrofluoric acid (HF). For heavy doping of the source and drain terminals, nonsource/drain areas were covered with a PR layer, then phosphorus ion implantation (5×10^{15} ions cm^{-3}) was performed at 30 keV. The wafers were annealed at 900 °C for 1 h to activate the dopants. A layer of Si_3N_4 (300 nm) was deposited on the wafers via physical evaporation for passivation. PR was coated over the wafer except on the areas reserved for the source and drain contact pads, and then the passivation layer over the contact pads was removed using ICP etch (TCP 9600, Lam Research). Layers of Ni (15 nm) and Ti (15 nm) were deposited over the source and drain using physical vapor deposition (PVD). Rapid thermal annealing was performed at 400 °C for 15 min to achieve reliable metal−Si ohmic contact via metal silicide formation. Unreacted Ni and Ti were removed using H_2SO_4 etching. Finally, the passivation layer (Si_3N_4) over the SiNWs was removed by coating non-SiNW areas with PR followed by ICP (TCP 9600). The final dimensions of the SiNWs in the single-SiNW FET devices and multi-SiNW FET devices were ~200 nm × 3 μm and 50 nm × 50 μm (width × length), respectively. Figure S1 (in Supporting Information) shows the scanning electron microscope (SEM) images of single- and multi-SiNW FET devices. The total number of SiNWs in the multi-SiNW FET devices was 26, resulting in a total width of ~48 μm (including the spaces between the NWs).

Polystyrene cloning cylinders (4.7 mm inner diameter ×8 mm height, Scienceware, Bel-Art), which served as cell culture chambers, were attached on the SiNW FET chips using polydimethylsiloxane (PDMS; Sylgard 184 Silicone Elastomer Kit, Dow Corning) as a glue. PDMS caps were also fabricated to cover the cloning cylinders with cells during electrical measurements. The PDMS glue and caps were prepared according to manufacturer's instructions.

Poly-D-lysine (PDL; Mw 70 000−150 000, Sigma-Aldrich) was immobilized in the areas enclosed by cylinders using (3-aminopropyl)-trimethoxysilane (APTMS; Sigma-Aldrich) as the linker molecule. To form an APTMS self-assembled monolayer (SAM) on the SiNW FET devices, chips were first cleaned with deionized (DI) water and 95% ethanol and then immersed in a 1% ethanolic solution of APTMS for 1 h at room temperature (RT). After SAM formation, the chips were rinsed with 99.9% ethanol twice to remove excess silane reagent. The chips were then heated in a 60 °C oven for 5 min to aid in further formation of siloxane bonds. For PDL immobilization, *N*-ethyl-*N*′-(3-(dimethylamino)propyl)carbodiimide (EDC; Sigma-Aldrich), *N*-hydroxysuccinimide (NHS; Sigma-Aldrich; EDC−NHS ratio = 4:1, total concentration = 10 mg/mL), and PDL (100 μg/mL) were dissolved in citrate buffer solution (CBS, pH 5.0). The APTMS-modified chips were then immersed in the PDL/EDC/NHS solution for 2 h at RT to allow the carbodiimide coupling reaction to complete. APTMS/PDL-modified surfaces were washed with phosphate buffered saline (PBS, 0.01 M; Biowest) twice and stored at 4 °C while immersed in PBS until use.

2.2. Culture, Seeding, and Neuronal Differentiation of PC12 Cells. PC12 cells (ATCC CRL-1721) were cultured in a growth medium consisting of the following: Roswell Park Memorial Institute (RPMI) 1640 medium with L-glutamine (85% v/v), horse serum (HS, 10% v/v), fetal bovine serum (FBS, 5% v/v), 4-(2-hydroxyethyl)-1-piperazineethanesulfonic acid buffer (25 mM), sodium pyruvate (1 mM), and penicillin−streptomycin (100 U/ml). All media reagents were acquired from Life Technologies. The cells were maintained in a 37 °C incubator with 5% CO_2 until use. Medium was changed every 2−3 d and passaged upon reaching 80% confluency.

The medium for PC12 differentiation was composed of RPMI 1640 medium with L-glutamine (85% v/v) and nerve growth factor (NGF;

DOI: 10.1021/acsami.5b01878
ACS Appl. Mater. Interfaces 2015, 7, 9866−9878

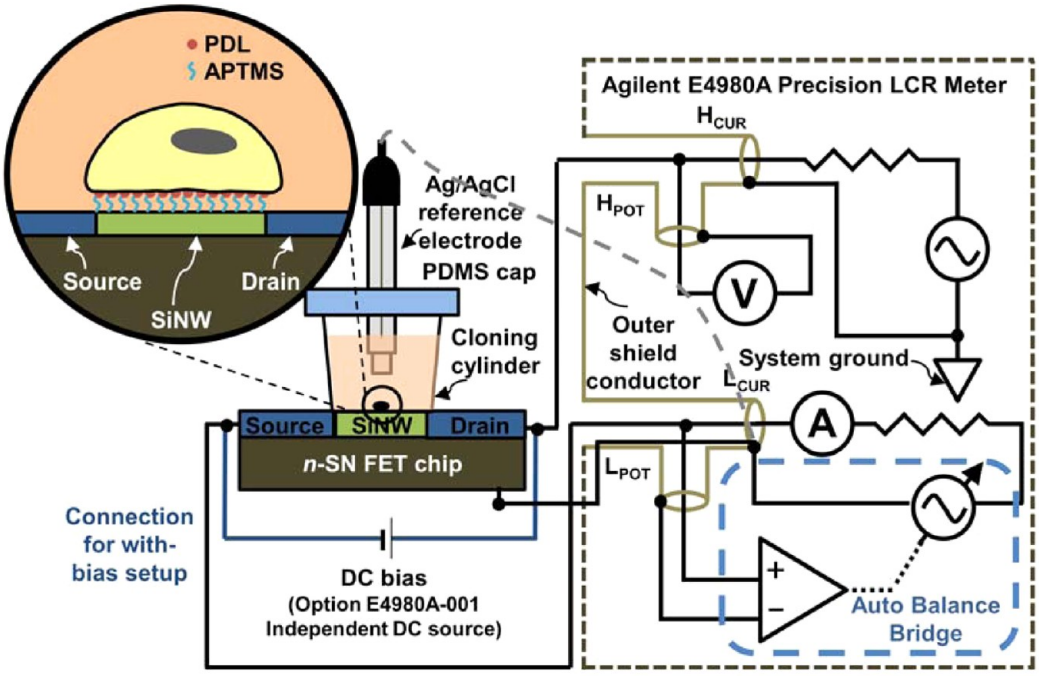

Figure 1. Non-Faradaic EIS measurement setup for monitoring PC12 cell growth and neuronal differentiation. PC12 cells were seeded on APTMS/PDL-modified SiNW FET devices. Changes in the impedance of the cell−SiNW FET system were determined using a precision LCR meter connected to the source and drain terminals of the SiNW FET device. A Ag/AgCl reference electrode was used as a solution gate. A LabVIEW program was used to control the LCR meter and to record the impedance data. (Note: Components in the figure are not drawn to scale.).

10 ng/mL; NGF-2.5S from murine submaxillary gland, Sigma-Aldrich).

Cell growth and neuronal differentiation of PC12 cells were monitored in the APTMS/PDL-modified chips with cylinders described above. PC12 cells (~45 000) in growth medium (100 μL) were seeded in each cylinder, resulting in a cell density of ~2.5 × 10^5 cells/cm^2. For PC12 neuronal differentiation, the cells were first cultured in growth medium for 24 h before starting differentiation in the NGF-supplemented medium. After every measurement, half of the growth/differentiation medium was replaced with fresh medium, and then cells were placed in a 37 °C incubator with 5% CO_2. At the end of the observation period, the differentiated PC12 cells were washed with DI water to cause osmotic-stress-induced cell death.

As a control for the cell growth experiment, we encapsulated PC12 cells in a three-dimensional (3D) scaffold composed of a poly(ethylene glycol) diacrylate (PEGDA) hydrogel. The PEGDA matrices, which were solidified on the surface of the SiNW FET devices, created an indirect contact between the PC12 cells and the SiNWs, but allowed the permeation of growth medium because of its porous structure and hydrophilic nature. The formulation of the PEGDA hydrogel used for the control samples was similar to that described in our previous study,[9] with some modifications. The hydrogel in this study consisted of the following: PBS (20% v/v), PEG (13.3% w/v; Mw 3,350, Sigma-Aldrich), PEGDA (66.7% w/v; Mw 700; Sigma-Aldrich), triethanolamine (100 mM; Alfa Aesar), and 2,2-dimethyl-2-phenyl-acetophenone (Sigma-Aldrich) in 1-vinyl-2-pyrrolidone (600 mg/mL, 4% v/v; Sigma-Aldrich). Growth medium and PDL (100 μg/mL) were added in the PEGDA precursor solution (medium−precursor solution ratio = 1:1). PC12 cells were added in PEGDA/medium/PDL precursor solution, resulting in a cell density of ~1 × 10^7 cells/mL. Cross-linking of the hydrogel on the devices was performed by exposure of the solution to a 23 W visible light source for 5 min.

2.3. Non-Faradaic EIS of the Cell−SiNW FET System. Before monitoring cell-related phenomena, we first performed impedance measurements with a SiNW FET device before surface modification, after APTMS modification, and after immobilization PDL to qualitatively confirm the success of each step-modification process. We measured the impedance for each condition in three different environments (air, DI water, and growth medium) to determine if the modification layers would influence the response of the devices to charged species in the measurement media.

Monitoring of PC12 cell growth was performed by measuring impedance changes in single-SiNW FET devices during a culture period of 5 d. Before measurements were performed for the cell cultures, impedance measurements were first performed after APTMS/PDL modification in growth medium. After PC12 cells were seeded, impedance measurements were performed at Days 0, 1, 3, and 5 postseeding. Day 0 measurement was performed 5 h after cell seeding. A total of three SiNW FET devices were used. The same measurement procedures were followed for the cell-laden PEGDA hydrogel.

For PC12 neuronal differentiation, monitoring was performed by measuring impedance changes in multi-SiNW FET devices during a differentiation period of 7 d. Before impedance measurements were performed for the differentiated cells, the impedance of the SiNW FET devices after APTMS/PDL modification in growth medium was first measured. After the growth medium was replaced with differentiation medium, impedance was measured at Days 0, 1, 2, 4, 5, and 7 after initial NGF treatment. Day 0 measurement here was performed right after exposure of cells to differentiation medium. After Day 7 measurements, impedance measurements were performed after cell death was induced among the differentiated PC12 cells by DI water. A total of three devices were used for monitoring PC12 differentiation.

Impedance measurements were performed using E4980A precision LCR meter (Agilent Technologies) in frequency sweep mode. Agilent E4980A was operated at 2 mV_{RMS} with a frequency range of 20 Hz to 2 MHz. Frequency sweep was performed with 100 sample points with log 10 scale. The LCR meter was connected to the SiNW FET devices using a four-terminal pair configuration: the high-current/high-potential and low-current/low-potential paired terminals were connected to the source and drain terminals, respectively, via coaxial cables. The SiNW FET devices were operated with a bias voltage of 10 mV in the subthreshold region, which has also been shown to provide the optimal sensitivity for nanowire FET biosensors.[36,37] A Ag/AgCl reference electrode was used as a solution gate to minimize external

DOI: 10.1021/acsami.5b01878
ACS Appl. Mater. Interfaces 2015, 7, 9866−9878

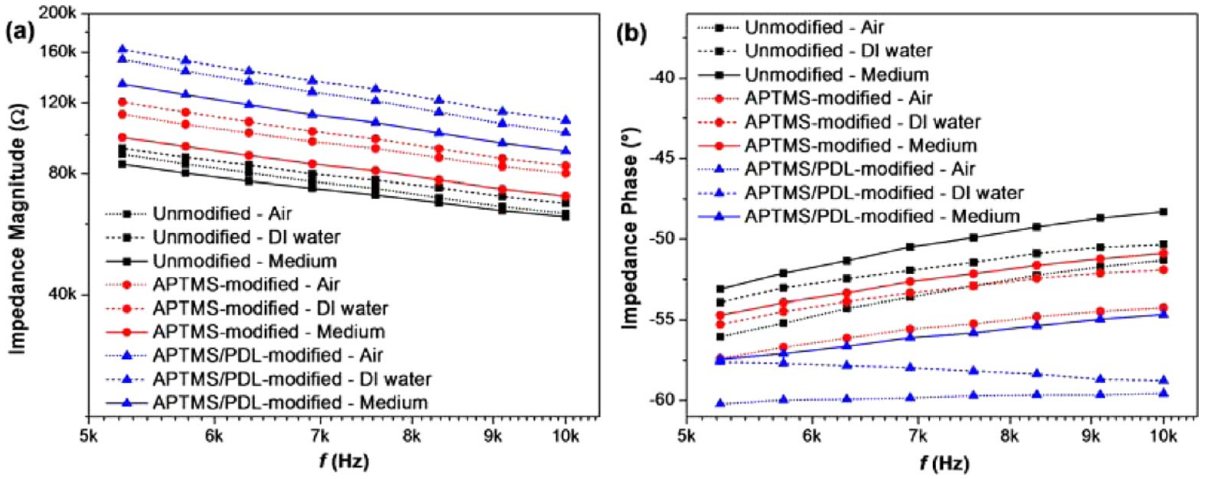

Figure 2. Bode plots of impedance magnitude (a) and impedance phase (b) for a representative SiNW FET device in air, DI water, and growth medium before surface modification, after APTMS modification, and after PDL immobilization. The distinguishable signals can be seen in impedance spectroscopy over the frequency span from 5 to 10 kHz.

noise. A LabVIEW program in a computer was used to control the settings of the LCR meter and to record the data for both impedance magnitude and impedance phase. Figure 1 shows an illustration of the impedance measurement setup for monitoring PC12 cell growth and neuronal differentiation.

Analysis for statistical significance of the means was performed using one-way analysis of variance (ANOVA) with Bonferroni's test.

2.4. Microscopic Observation of PC12 Cells. For microscopic observation of PC12 cell growth and neuronal differentiation, cells were seeded on SiNW FET chips and cultured for 5 and 7 d, respectively. After the culture period, the PC12 cell growth and differentiation samples were first washed with PBS twice and then fixed with 2.5% glutaraldehyde for 1 h. The fixed cells were dehydrated by immersion in a graded series of ethanol (20 min each). Finally, the dehydrated samples were coated with gold using a sputtering coater and then observed using a field emission scanning electron microscope (FESEM; JSM-6700F, JEOL).

To visualize the direct contact between undifferentiated/differentiated PC12 cells and SiNWs and PC12 cell growth in the PEGDA hydrogel, cells were further examined by fluorescence microscopy. Cells were fixed with 4% paraformaldehyde for 1 h and stained with 1 ng/mL 4′,6-diamidino-2-phenylindole (DAPI; Millipore) and 0.4 U/mL rhodamine phalloidin (RP; Millipore) in 1% bovine serum albumin (BSA) in PBS for 1 h. Cells were then immunochemically stained with mouse antivinculin monocolonal antibody (1:200, Millipore), followed by FITC-conjugated antimouse secondary antibody (1:200, Millipore). Samples were washed twice with 1% BSA/PBS and examined under confocal laser scanning microscopes. Visualization of the direct contact on SiNW was examined using Leica SP5 upright confocal microscope, and observation of PC12 cell growth in the PEGDA hydrogel was performed using Carl Zeiss LSM 510 inverted confocal microscope.

3. RESULTS AND DISCUSSION

The impedance measurement setup employed in this study provides a direct measurement of the electrical characteristics of the SiNW FET device itself while applying a bias voltage between source and drain. The electrical characteristics of immobilized substances and/or solution are probed by means of the potentiometric gating effect of their charged species on the SiNW channel. Total impedance (Z) can be expressed in terms of the impedance magnitude ($|Z|$) and impedance phase (θ), where a voltmeter and an ammeter generally measure vectors (magnitude and phase angle) of the signal voltage and current, respectively. The impedance magnitude and impedance phase at varied frequencies are measured by the LCR meter in this study using the autobalancing bridge method. The detailed definitions and illustrations regarding non-Faradaic impedance values can be found in Supporting Information. The LCR meter measurement setup provides a simple means of probing the adhesion and spreading of anchorage-dependent cells, which can serve as indicators of cell viability and changes in morphology according to the equivalent electric circuit of the cell−biosensor system, as what has been done in other impedance spectroscopy studies using cell-based FET devices.[13,17,27] Aside from these applications in probing cell conditions, the nanoscale interfaces of modified biomolecules and SiNW as well as of cells and biomolecules, can be explored using EIS by observing the changes in the values of the equivalent electric components.[9]

3.1. Effect of Nanoscale-Modified Surfaces on Impedance. In a cell-based biosensor, effective transduction of a signal or condition of the coupled cell necessitates good interfacing between the biological component and the sensing element. For instance, a strong, tight seal between a neuron and an electrode is ideal to prevent leakage of currents into the surrounding medium[9,12] and to prolong the functional activity of the sensor.[17] To promote cell adhesion, sensor surfaces are usually surface-modified with extracellular matrix (ECM) components,[38,39] polycationic molecules,[29,40,41] or adhesion ligands.[42] In this study, we induced cell adhesion onto the SiNW FET surface using covalently immobilized PDL, a polycationic molecule commonly used for the surface treatment of tissue culture plates. It is believed that polylysine promotes cell adhesion through its primary amine groups, which bear a positive charge ($-NH_3^+$) in aqueous solutions with physiological pH;[43,44] the overall positive charge results in electrostatic attraction of negatively charged cell membranes.[44,45] Although PDL may not directly associate with cell adhesion molecules, it has the advantages of reducing interference with cell physiology owing to its synthetic nature and withstanding proteolytic cleavage because of its D-enantiomeric configuration.[41] Covalent immobilization of PDL was favored over adsorption to create a tighter junction that can withstand motility forces exerted by cells.[39]

In our previous study,[45] we verified the successful covalent immobilization of PDL or poly-L-lysine (PLL) on our fabricated

DOI: 10.1021/acsami.5b01878
ACS Appl. Mater. Interfaces 2015, 7, 9866−9878

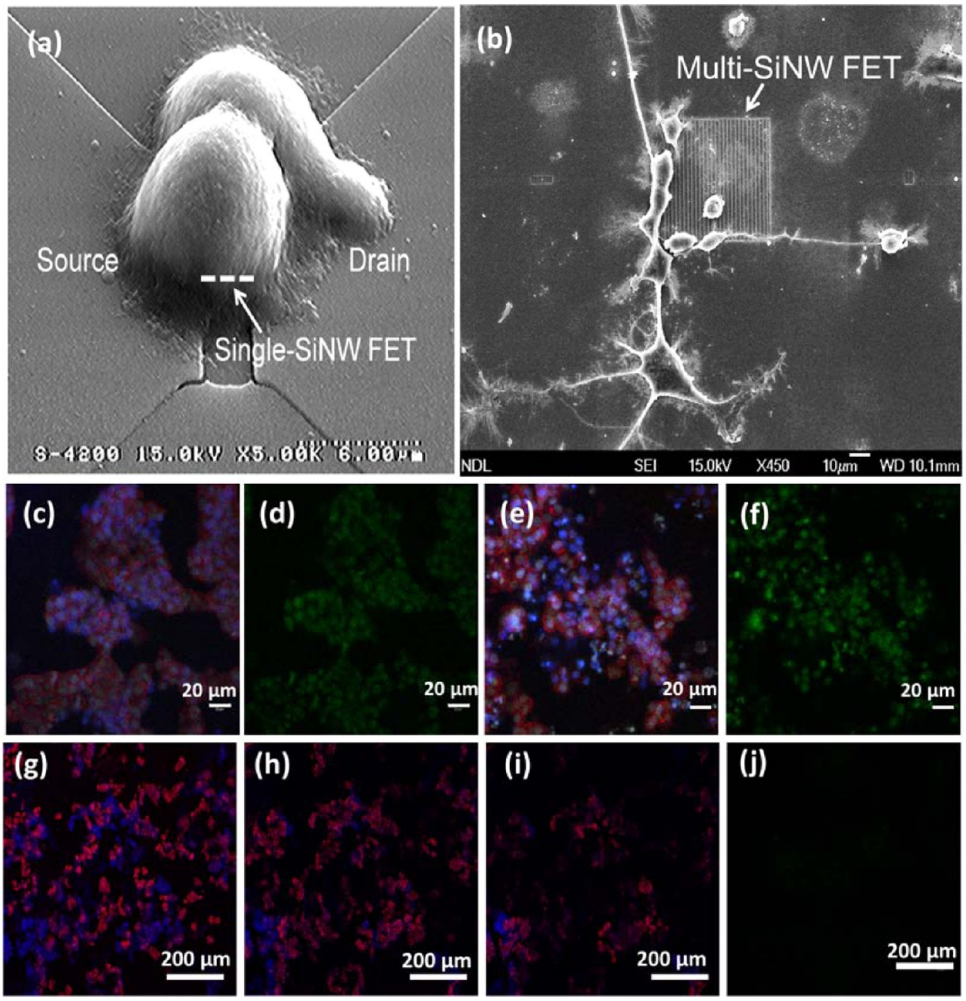

Figure 3. Microscopic observation of cell conditions. (a) An SEM image of a PC12 cell attached on a single-SiNW FET device after 5 d of culture. The single-SiNW channel beneath the PC12 cell is drawn for illustration. (b) An SEM image of differentiated PC12 cells on a multi-SiNW FET device after 7 d in differentiation medium. (c)−(j) The results of fluorescent examination of undifferentiated/differentiated cells on SiNW FETs and 3D cell growth in PEGDA hydrogel. (c) and (e) RP and DAPI fluorescent staining (red and blue, respectively) with antivinculin expression (green) of undifferentiated and differentiated cells, respectively. Antivinculin staining of undifferentiated and differentiated cells on single-SiNW and multi-SiNW are displayed in (d) and (f), respectively. PC12 cells cultured in a PEGDA hydrogel at the top (g), middle (h), and bottom (i) portions of a ∼100 μm thick slice of the scaffold are also shown. Fluorescent staining for vinculin expression did not appear at the bottom of hydrogel in close proximity with the sensing area (j). RP- and DAPI-stained areas represent the actin-rich cytoskeletons and nuclei, respectively, of the PC12 cells. The cells were seeded at a density of $\sim 1 \times 10^7$ cells per cm^3 of the hydrogel.

SiNW FET devices via APTMS coupling using electron spectroscopy for chemical analysis and PLL−fluorescein isothiocyanate staining. The APTMS/PDL-modified SiNW FET chips supported the growth and proliferation of PC12 cells, which proves that such surface modification imparted a functional biointerface to the devices. In this study, we confirmed the successful modification of the SiNW FET devices with APTMS and with APTMS/PDL using the changes in the impedance of the devices after each step-modification. Figure 2 shows the frequency-sweep impedance data for air, DI water, and growth medium before and after surface modification with an APTMS SAM and covalent attachment of PDL molecules. The frequency range of ∼5−10 kHz is shown because greater signal difference was observed in this range based on the full impedance spectra (Figure S2, in Supporting Information). It can be seen that the impedance magnitude consistently increased in the order of growth medium, air, and DI water for all surface modification conditions between ∼5−10 kHz. On the other hand, impedance phase consistently became more negative in the order of growth medium, DI water, and air for all surface modification conditions in this frequency range. The increase in impedance magnitude and negative shift in impedance phase for all environments after each modification step are probably due to the increasing thickness of the modification layers on the SiNW FET devices. These layers resulted in a capacitive contribution to the overall impedance as can be inferred from the shift of the impedance phase to more negative values. This capacitive layer can also be viewed as an insulating layer that reduced the potentiometric gating effect of free ions in the environment on the SiNW channel, leading to a decrease in local carrier concentration and an increase in impedance magnitude.

Despite the apparent screening effect caused by the increasing thickness of the modification layers, it can be seen from the graphs in Figure 2 that the unmodified, APTMS-modified, and APTMS/PDL-modified SiNW FET devices can still effectively distinguish between ion concentrations in an

DOI: 10.1021/acsami.5b01878
ACS Appl. Mater. Interfaces 2015, 7, 9866−9878

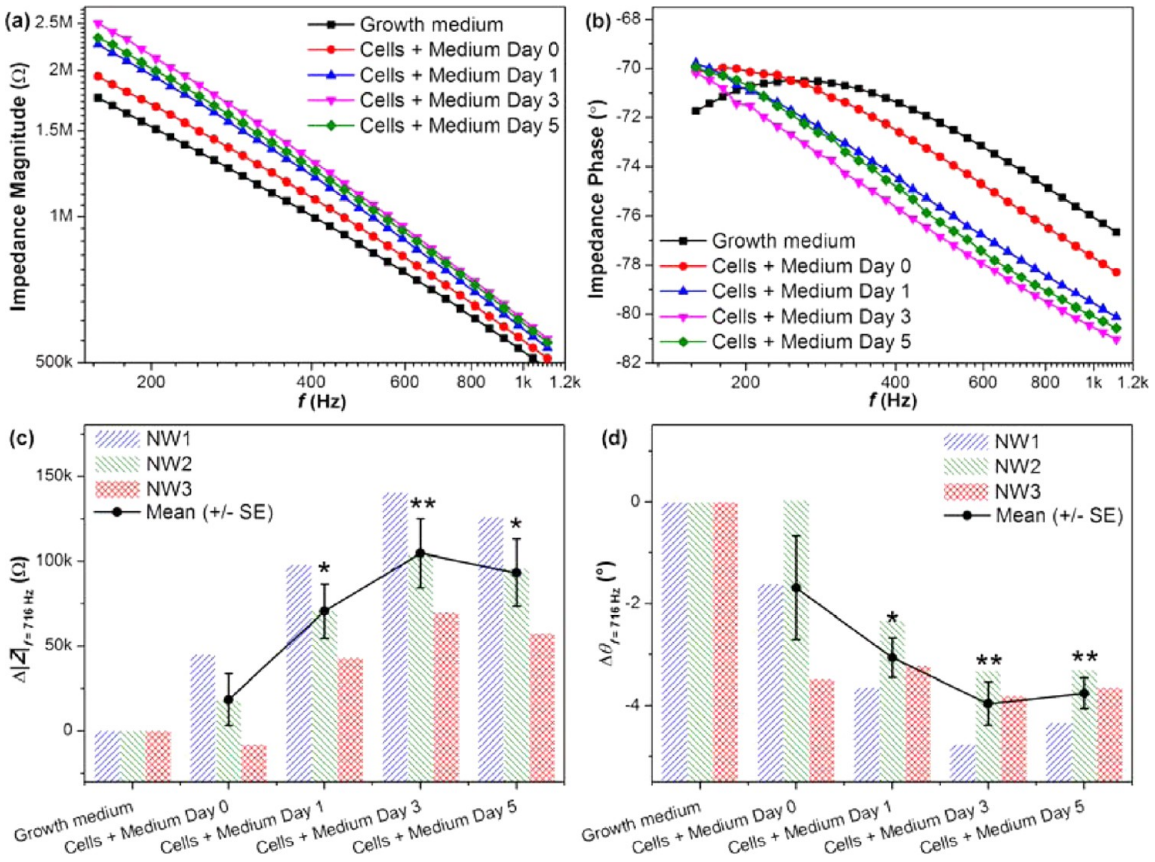

Figure 4. Impedance spectroscopy for observation of cell growth. Bode plots of impedance magnitude (a) and impedance phase (b) are shown for a representative SiNW FET device during PC12 cell growth for 5 d. Changes in impedance magnitude (c) and impedance phase (d) of different SiNW FET devices (n = 3) were analyzed at an input frequency of 716 Hz. Average values are plotted as a line to show the apparent trend in the impedance parameters. (*p < 0.05; **p < 0.01; the statistical significance is relative to the condition of cells in medium at Day 0).

environment. The higher concentration of charged species (dissociated inorganic salts, amino acids, proteins) in the growth medium resulted in a lower impedance magnitude and less negative impedance phase for medium than for DI water and air in all the devices. In addition, the difference in impedance magnitude between air and growth medium is greater than that between air and DI water, especially in APTMS-modified and APTMS/PDL-modified devices. This shows the ability of the devices to correctly distinguish between environments of different ionic concentrations. This also confirms the successful surface modification with APTMS and APTMS/PDL, which should improve the affinity of the modified surface to charged species because of existence of protonated amine groups.[46] These results are consistent with our previous findings that the changes in output voltage of a SiNW FET measurement system were greater in PBS (at different pH values) than in DI water relative to air, and that APTMS-modified SiNW FET devices give greater signal changes than unmodified devices.[35]

3.2. Microscopic Observation of Cell Conditions. The PC12 cell line, which is a well-known model system for neural cells and neuronal differentiation, was used for monitoring cell adhesion. PC12 cells were chosen because neuronal differentiation was also intended to be performed for sensing of morphological changes in cells. Figure 3a,b shows the SEM images of a representative single-SiNW FET device interfaced with a PC12 cell and a representative multi-SiNW FET device interfaced with differentiated PC12 cells, respectively. It can be seen that the PC12 cell is firmly attached on the APTMS/PDL-modified device after 5 d of culture in Figure 3a. The differentiated PC12 cells cultured for 7 d appear significantly more flattened in Figure 3b compared with the undifferentiated PC12 cells (Figure 3a). In addition to the neurites extending from the PC12 soma, this characteristic flat morphology of differentiated PC12 cells contribute to greater coverage of the multi-SiNW structure.

Because of the high ionic concentration of growth medium, the Debye–Hückel length is ~1 nm in this study. If the sensing principle relies on the surface charges of the cells, it means that the cell–SiNW junction should be very tight. Further examination of direct contact between undifferentiated/differentiated PC12 cells and SiNWs and PC12 in PEGDA hydrogel and SiNWs was performed, as shown in Figures 3c–j. Immunostaining with monoclonal antivinculin antibody was performed (Figures 3c–f) to demonstrate the direct contact between cells and sensing areas. In Figure 3d,f, vinculin expression (green fluorescence) shows that both undifferentiated and differentiated PC12 cells firmly anchored onto the surfaces of sensing devices, either single-SiNW or multi-SiNW, through integrins.[39,44] Furthermore, the vinculin fluorescence confirms a larger contact area of differentiated PC12 cells (Figure 3f) in comparison with undifferentiated cells (Figure 3d).

To confirm if the changes in impedance parameters during PC12 cell adhesion are due to the negatively charged cell membrane and screening of charges in the solution, we

DOI: 10.1021/acsami.5b01878
ACS Appl. Mater. Interfaces 2015, 7, 9866–9878

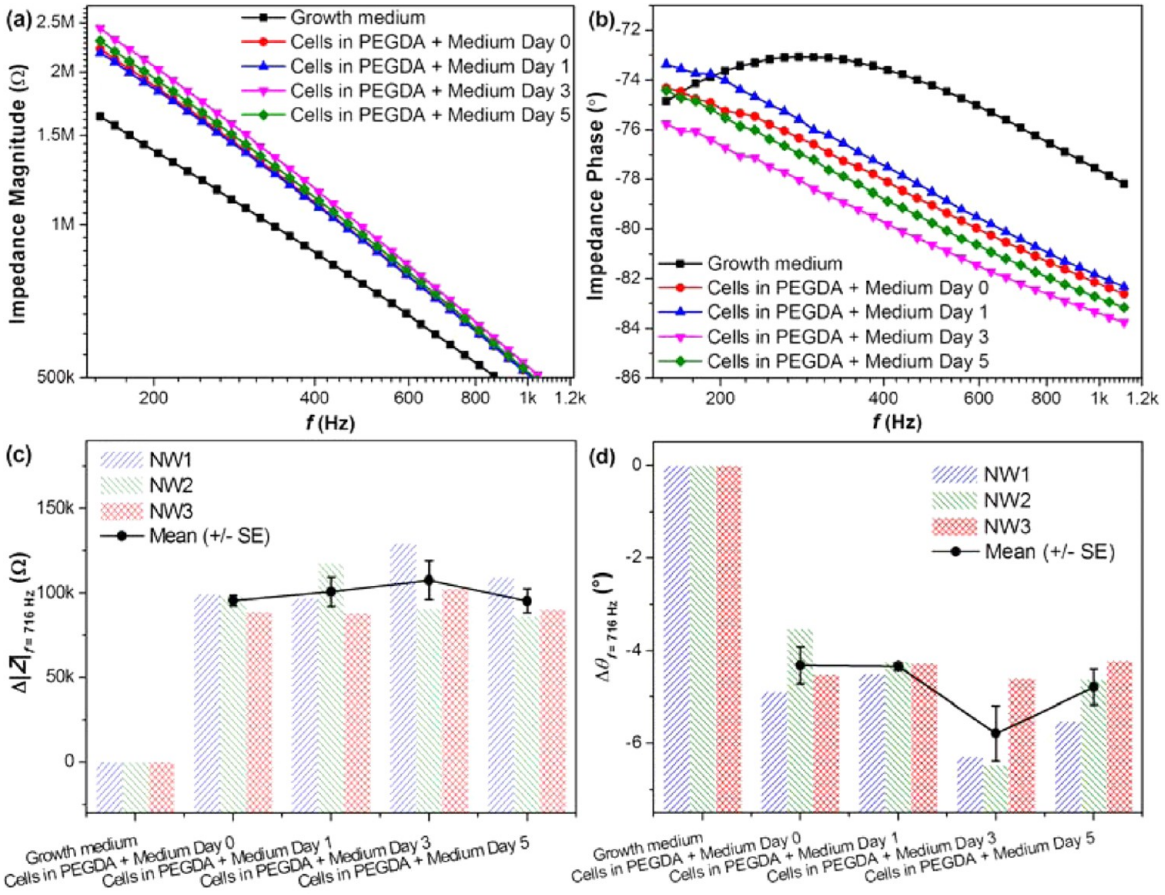

Figure 5. Verification of impedance spectroscopy of cell growth using PC12 cells embedded in a PEGDA hydrogel. Bode plots of impedance magnitude (a) and impedance phase (b) are shown for a representative SiNW FET device during measurement with the cell-laden PEGDA hydrogel for 5 d. Changes in impedance magnitude (c) and impedance phase (d) of different SiNW FET devices (n = 3) were analyzed at an input frequency of 716 Hz. Average values are also plotted as a line to show the apparent trend in the impedance parameters.

encapsulated PC12 cells in a 3D scaffold composed of a PEGDA hydrogel. The hydrogel scaffold encapsulated the cells, preventing their direct contact with the SiNW FET devices. But the scaffold encouraged permeation of the growth medium because of its high porosity and high wettability.[9] Thus, the cell-laden PEGDA hydrogel served as a convenient control by allowing us to both prevent cell adhesion and investigate the effect of growth medium on the impedance of the SiNW FET devices. PEG-derived hydrogels have been shown to support cell growth,[9,47] and in this study, we also observed PC12 proliferation in the 3D PEGDA hydrogel using confocal fluorescence microscopy with RP and DAPI staining in Figure 3g–i. However, staining for vinculin expression did not show the characteristic green fluorescence at the bottom of the hydrogel (in Figure 3j), where the sensing devices were located. A video of the fluorescence observation of a 100 μm thick slice of the cell-laden hydrogel scaffold is included in the Web site ("PC12 in PEGDA Hydrogel.avi").

3.3. Changes in Impedance during PC12 Cell Growth.

Observation of cell adhesion during growth on sensing elements is usually a preliminary step in the impedimetric monitoring of the effect of drugs on cells.[11,13,27] This is performed not only to establish a baseline data against with subsequent changes caused by the drugs can be compared, but also to ensure that viable, functional cells exist on the sensor surface. After the successful covalent immobilization of PDL on the SiNW FET devices, we confirmed the creation of a functional biointerface by seeding PC12 cells and monitoring SiNW FET impedance changes that may be correlated with the attachment and growth of the cells. Figure 4 shows the Bode plots and time-course graphs of impedance magnitude and impedance phase during PC12 cell growth on the SiNW FET devices for 5 d. On the basis of the full impedance spectra (Figure S3, in Supporting Information), significant changes in the impedance parameters can be observed in the lower frequency range (~150 Hz–1 kHz), as shown in the representative graphs in Figure 4a,b. In particular, based on the three SiNW FET devices that were used, the largest impedance changes occurred at ~716 Hz; thus, we used the impedance values at 716 Hz to monitor time-dependent PC12 cell growth, as shown in Figures 4c,d. Note that the actual impedance values are shown in Figure 4a,b, while the change in impedance magnitude ($\Delta|Z|$) and impedance phase ($\Delta\theta$) with respect to growth medium value (baseline) are shown in Figure 4c,d. To better visualize the trend in signal changes, Figure 4c,d show a trendline with points and error bars corresponding to the mean and the standard error of the mean (SE), respectively. It can be seen that error bars in the trendlines are relatively large; however, the trends in signal changes still appear consistent for almost all SiNW FET devices. The sample-to-sample signal variations may be attributed to variations in device fabrication, APTMS/PDL modification, and/or cell/NW interfacing.

DOI: 10.1021/acsami.5b01878
ACS Appl. Mater. Interfaces 2015, 7, 9866–9878

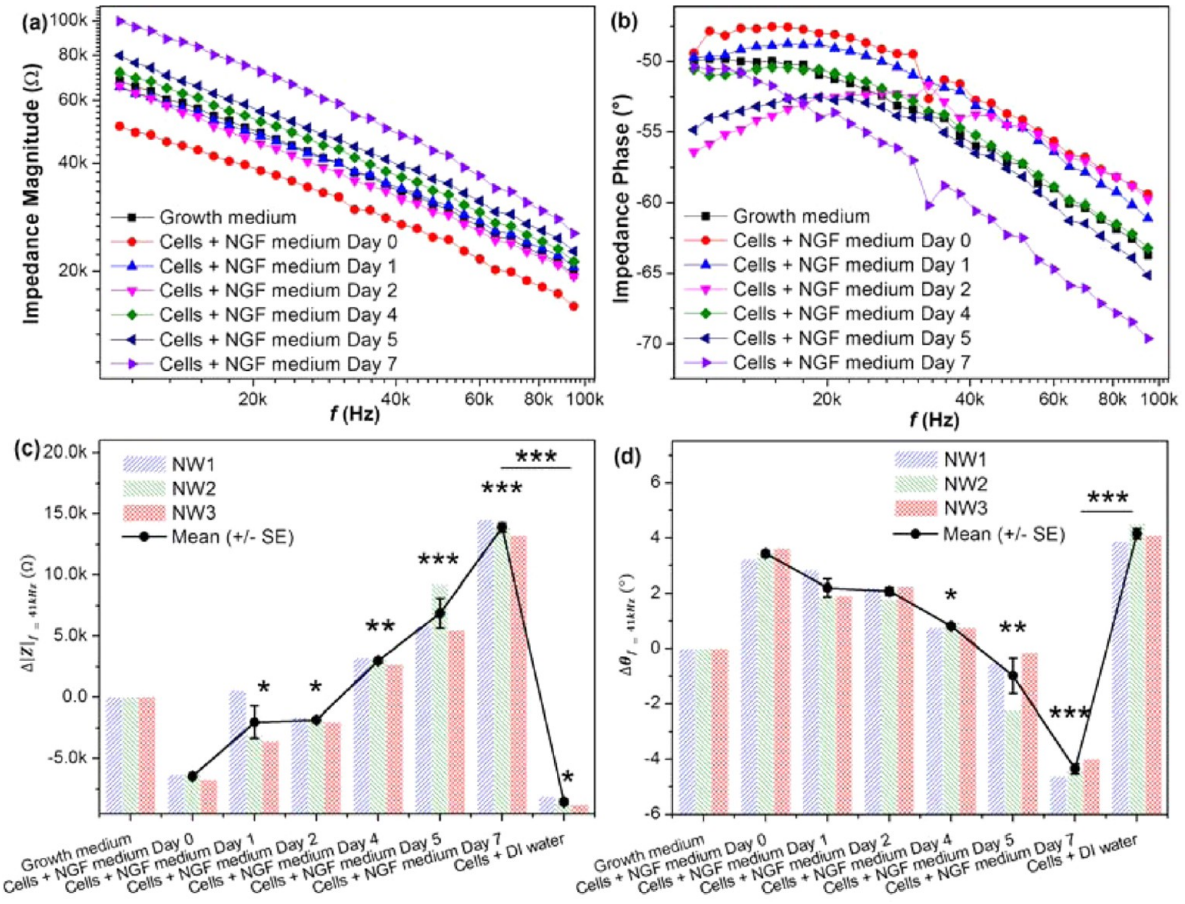

Figure 6. Impedance spectroscopy for observation of cell differentiation. Bode plots of impedance magnitude (a) and impedance phase (b) are shown for a representative SiNW FET device during PC12 neuronal differentiation for 7 d. Changes in impedance magnitude (c) and impedance phase (d) of different SiNW FET devices ($n = 3$) were analyzed at an input frequency of 41 kHz. Average values are also plotted as a line to show the apparent trend in the impedance parameters. ($*p < 0.05$; $**p < 0.01$; $***p < 0.001$; the statistical significance is relative to the condition of cells in NGF medium at Day 0 and between "cells + DI water" and "cells in NGF medium at Day 7").

As can be seen in Figures 4c,d, there is an increase in the impedance magnitude and a negative shift in the impedance phase after seeding the PC12 cells on the devices. As the culture d progressed, the impedance magnitude continued to increase, and impedance phase continued to shift to more negative values, with both parameters reaching a plateau 3 d after cell seeding. The observed increase in the impedance magnitude after cell seeding might be due to either the coupling of the negatively charged cell membrane with the SiNW channel or the shielding of the SiNW from charged species in the medium by the attached cell. The observed increase in the impedance magnitude after cell seeding can be attributed to the overall negative charge of cell membranes: when the cells firmly attached onto the SiNW FET devices (in Figures 3a,c,d), the negatively charged membranes repelled the electrons (majority carriers) in the *n*-type SiNW channel, leading to a decrease in local carrier concentration and an increase in impedance magnitude. A previous study has confirmed this net negative surface charge on the plasma membrane of PC12 cells, attributing such charges to monovalent acidic functional groups.[48] On the other hand, the screening of charges by cell coverage resulted in a reduced potentiometric gating effect on the SiNW. As can be seen in Figure 4d, the impedance phase shifted to more negative values as the culture period progressed, which is indicative of increasing dominance of capacitance. This was probably due to the increasing capacitive contribution of the cell membrane during cell growth on the devices, in addition to the capacitive effect of the immobilized molecules on the SiNW surface, as earlier described.[10−12,48] The continued changes in the impedance parameters until Day 3 might have been caused by the flattening of the PC12 cells in a planar culture, a phenomenon that has also been observed in other anchorage-dependent cells.[49,50] In this study, the PC12 cells began to slightly flatten even only after 24 h postseeding (Figure S4, in Supporting Information). Alternatively, the changes in impedance parameters can also be explained by a decrease in the distance of interface between the cell membrane and the SiNW, which leads to a higher seal resistance.[9,17] This could have occurred in the experiment since flattening of cells can indicate improved cell adhesion.[9,17,51,52] However, PC12 cells can only flatten to a certain extent, if not induced to differentiate to the neuronal phenotype. This might be the reason why the impedance changes appeared to have stabilized 3 d after cell seeding.

To confirm if the changes in impedance parameters during PC12 cell adhesion are due to the negatively charged cell membrane and screening of charges in the solution, PC12 cells were encapsulated in a 3D PEGDA hydrogel in SiNW FET devices. Figure 5 shows the Bode plots and time-course graphs of the impedance parameters during measurements with the 3D cell culture in PEGDA hydrogel for 5 d. On the basis of the full impedance spectra (Figure S5, in Supporting Information), the

DOI: 10.1021/acsami.5b01878
ACS Appl. Mater. Interfaces 2015, 7, 9866−9878

largest signal changes resulting from cell-laden PEGDA hydrogel are in the lower frequency range, as shown in Figure 5a,b. In Figure 5c,d, the graphs of impedance magnitude and impedance phase for three SiNW FET devices are shown for the frequency 716 Hz. This frequency is the same as the one used for the analysis of two-dimensional (2D) PC12 cell growth and is within the frequency range where signal changes can be observed (Figure 5a,b). It can be seen that the SiNW FET devices showed an abrupt increase in impedance magnitude and negative shift in impedance phase after photopolymerization of the PEGDA hydrogel on the chip. The sudden negative shift in impedance phase is due to the addition of a capacitive layer of hydrogel on the SiNW FET devices. Therefore, the significant initial changes in the impedance parameters after addition of the cell-laden PEGDA hydrogel on the devices were probably due to the screening of charged species in the surrounding medium. In the following days, both impedance magnitude and impedance phase did not show significant changes. This is unlike the gradual changes observed during 2D PC12 cell culture on the SiNW devices. On the basis of the sparse distribution of PC12 cells in the hydrogel (Figure 3i) and the indirect contact with SiNW (Figure 3j), the difference in the trends of impedance parameters for PC12 cell culture in 2D and 3D environments is because the cells in the PEGDA hydrogel were not in direct contact with the SiNW FET devices. On the other hand, Bode plots of $|Z|$ and θ for representative SiNW FET devices with blank PEGDA hydrogels measured for 5 d are shown in Figure S6 (in Supporting Information). It can be seen that the $\Delta|Z|$ and the $\Delta\theta$ plots for the blank hydrogel samples also demonstrated the same trends as the 3D cultures. Consequently, the PC12 cells embedded in the PEGDA hydrogel did not influence the impedance measurements for the 3D cultures.

3.4. Changes in Impedance during PC12 Neuronal Differentiation. After confirming that SiNW FET devices can successfully monitor the adhesion of cells during cell growth, we tested the feasibility of using these devices to observe time-course morphological changes induced by exogenous agents on cells. For this, we also used PC12 cells and triggered their differentiation (or morphological change) using NGF as the exogenous agent. Multi-SiNW FET devices were used in the experiments instead of single-SiNW FET devices because of the larger sensing area available onto which PC12 cells can attach and spread during neuronal differentiation.

Figure 6 shows the Bode plots and time-course graphs of the impedance parameters during the seven-day neuronal differentiation of PC12 cells. The graphs in Figure 6a,b represents the frequency sweep spectra of the impedance magnitude and impedance phase, respectively, for the frequency range of 10–100 kHz, which is where the signal changes in impedance magnitude are more apparent based on the full impedance spectra (Figure S7, in Supporting Information). From these graphs, changes in both impedance magnitude and impedance phase appear to be more consistent above 40 kHz. We selected 41 kHz and plotted the time-course changes in the impedance parameters at this frequency for three SiNW FET devices, as shown in Figure 6c,d.

Figure 6c,d shows an initial decrease in impedance magnitude and positive shift in impedance phase at Day 0 of PC12 differentiation, which was different from what we observed when cells were seeded in the cell adhesion experiment. This can be mainly explained by the added NGF in the medium, which has a net positive charge at physiological pH,[53] although the removal of serum proteins may have also decreased the concentration of negatively charged species in the differentiation medium. After these initial changes in the impedance parameters, we see a consistently increasing trend in impedance magnitude and a shift to increasingly negative values in impedance phase in all three SiNW FETs utilized. The trends in the impedance parameters during PC12 differentiation in the first few days of culture are similar to those for 2D PC12 cell growth. This similarity is most likely due to the same causative phenomenon for the impedance changes, which is the negatively charged cell membrane and shielding of the SiNW channel from the charges in the surrounding medium by the cells. Nevertheless, an important difference between the time-course measurements in undifferentiated and differentiated PC12 cells is that the trends observed in the differentiated PC12 cells continue until Day 7, unlike those in undifferentiated PC12 cells, which already plateaued at Day 3. For differentiated PC12 cells, the continued trend in impedance parameters is consistent with the known morphological changes of PC12 cells in response to NGF, such as flattening, extension of neurites, and formation of neuronal networks, which reach completion after ~7 d of NGF exposure.[54] Our results indicate that the increased frequency shift after growth factor induction is due to distinctive morphological changes in the PC12 cells, giving rise to a larger coverage of the cell membrane on the SiNWs according to the antivinculin staining (Figure 3f).

At the end of the differentiation period, the PC12 cell culture was exposed to DI water to induce cytolysis. The original signal changes in impedance magnitude and impedance phase after DI water treatment are also shown in the full impedance spectra in Figure S7a,b, respectively (in Supporting Information). This osmotic-stress-induced cell death was expected to cause detachment of cells from the SiNW FET devices, which should restore the impedance values to their original preseeding levels. In Figure 6c,d, it can be seen that the impedance magnitude and impedance phase significantly decreased and became less negative, respectively. However, their values are significantly lower (or less negative for phase) compared with the values for growth medium, which is contrary to the expected higher impedance magnitude and more negative impedance phase for DI water, as can be inferred from Figure 2. These results indicate that the impedance changes were not caused by the different measurement solutions but by some other factors, which were most probably the detachment of dead cells and the rupturing of their cell membranes because of cytolysis. Cell detachment removed the influence of the negatively charged cell membranes on the SiNW channels, which would have restored the impedance levels to their preseeding values in growth medium. On the other hand, rupturing of the cell membranes released cell lysates such as proteins into the DI water. Since proteins can become charged, this might have caused the lower impedance magnitude and less negative impedance phase for DI water compared with the growth medium. Consequently, we can conclude that the trends in the impedance parameters during the culture period were indeed due to PC12 neuronal differentiation on the devices.

3.5. Interpretation of Impedance Changes for Different Cell Conditions Using Equivalent Circuits. One advantage of non-Faradaic EIS over optical approaches is the interpretation of measurements by modeling the interfacial effect of modified layers or the contacts between cells and

DOI: 10.1021/acsami.5b01878
ACS Appl. Mater. Interfaces 2015, 7, 9866–9878

sensing devices.[8−12,14,27] Impedance parameters obtained from non-Faradaic EIS were used in this study to investigate the interfacial effects of cell growth/differentiation on the SiNW FETs. According to the definition of impedance values in Supporting Information, resistance and capacitance are the main parameters affecting the impedance magnitude and phase. Table 1 shows the summary of observed trends in impedance parameters for surface-modified SiNW, direct PC12 cell contact, indirect PC12 cell contact (via PEG encapsulation), and PC12 cell differentiation. After surface modification, impedance magnitude increased, and impedance phase approached more negative values (Figure 2). Although it is the resistance from the modified SAM layer (R_s) that generally affects the impedance values, it seems that the SAM layer also contributed a capacitance (C_s) and had a large impact on the impedance phase. On the other hand, the impedance magnitude during PC12 proliferation (Figure 4) and differentiation (Figure 6) abruptly increased because cell adhesion and neurite outgrowth resulted in direct contact of the cell membrane with the sensing area. While the cells completely covered the modified SiNWs, cell membranes further contributed additional resistance and capacitance.[9−12,14] Changes in impedance magnitude could be easily distinguished at certain frequencies owing to the resistance and capacitance effects from cell membranes. By the same token, capacitance significantly affected the impedance phase, as can be seen in Figures 4 and 6. Figure 7 illustrates the equivalent electric components for the surface-modified SiNW, direct PC12 cell contact, indirect PC12 cell contact, and PC12 cell differentiation. A more detailed discussion of the theoretical equivalent electric circuit of the measurement setup consisting of a biological cell attached on an APTMS/PDL-modified SiNW FET can be found in Supporting Information (Figure S8).

Table 1. Summary of Observed Trends in Impedance Parameters

	impedance parameters			
	$\lvert Z\rvert$	θ	R_p[a]	C_p[a]
direct PC12 cell contact (5 d)	increasing then plateau	negative then plateau	increasing then plateau	decreasing then plateau
indirect PC12 cell contact (5 d)	almost no change	almost no change	almost no change	almost no change
PC12 cell differentiation (7 d)	increasing	more and more negative	increasing	decreasing

[a] R_p and C_p refer to a resistor and a capacitor model, respectively, connected in parallel.

A surface-modified SiNW can be represented by a parallel connected resistance (R_s) and capacitance (C_s) due to the SAM modification, as shown in Figure 7a.[9,27] For direct PC12 cell growth on the SiNWs, a variable resistance (R_c) and variable capacitance (C_c) is added, representing the interface between the cells and the modified SiNW.[9,10,14] The equivalent circuit

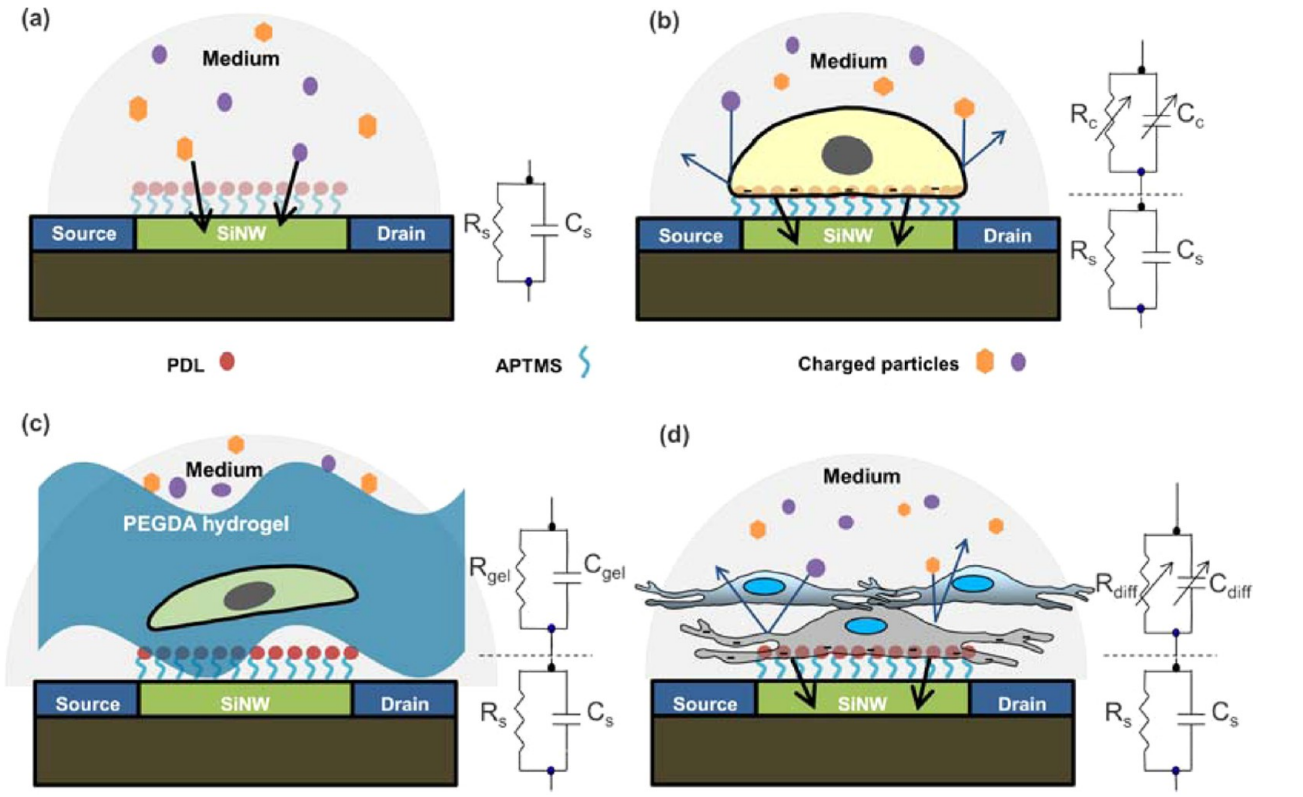

Figure 7. Equivalent electric circuit of the cell/SiNW interface. The sensing conditions and equivalent circuits are illustrated for the surface-modified SiNW (a), PC12 cell growth in direct contact with SiNW (b), indirect PC12 cell contact (c), and PC12 cell differentiation (d). The black arrows represent the dominant effects on the conductance of the SiNW. (R_s: resistance of SAM layer; C_s: capacitance of SAM layer; R_c: variable resistance of cell membranes during PC12 cell growth; C_c: variable capacitance of cell membranes during PC12 cell growth; R_{gel}: resistance of PEGDA hydrogel; C_{gel}: capacitance of PEGDA hydrogel; R_{diff}: variable resistance of cell membranes during PC12 differentiation; C_{diff}: variable capacitance of cell membranes during PC12 differentiation.).

DOI: 10.1021/acsami.5b01878
ACS Appl. Mater. Interfaces 2015, 7, 9866−9878

representing the parallel components R_s and C_s for the SAM modification and the variable R_c and C_c for the cell membranes of the undifferentiated PC12 cells covering the modified SiNWs (Figure 3a) is depicted in Figure 7b. Figure 7c shows the equivalent circuit for indirect cell contact under the condition of suspension cell growth in PEGDA hydrogel. The addition of PEGDA hydrogel resulted in large changes in impedance magnitude and phase at the start of the measurement because of R_{gel} and C_{gel}. However, the changes in impedance magnitude and phase had no obvious trends in the subsequent days because of the indirect contact between cells and modified SiNW. For the differentiation of PC12 cells, the equivalent circuit is shown in Figure 7d. Aside from the parallel R_s and C_s for the surface-modified SiNW, a parallel circuit of variable resistance R_{diff} and variable capacitance C_{diff} is included. The larger contact area of differentiated PC12 cells on the SiNWs prevented charged particles from directly affecting the conductivity of SiNW and resulted in significant changes in impedance values. The NGF treatment in the first 2 d resulted in significant changes in impedance magnitude but not in phase owing to R_{diff} from the contact area of the initially differentiated cell. Thereafter, increasing values of R_{diff} from well-differentiated cells further prevented the charged particles from reaching the SiNWs, and larger changes in impedance magnitude were recorded. The significant negative change in impedance phase at Day 7 for cell differentiation can be ascribed to C_{diff} due to the larger contact of the well-differentiated cells with the SiNW.

Our results show that non-Faradaic EIS has an advantage of simultaneously observing signals from SiNW FET devices over a wide frequency span in comparison with measurement at a certain fixed frequency.[32] It is apparent from Figure 6c,d that the changes in the impedance parameters and the variations of the data among the different devices used are much smaller for the multi-SiNW FET devices compared with the single-SiNW FET devices (Figure 4c,d). These differences are probably due to the larger exposed channel area in multi-SiNW, which might have helped in improving the coupling of the cells. Therefore, although single-SiNW FET devices are useful in probing individual cells, it seems that multi-SiNW FET devices yield better results for cell adhesion and cell spreading studies.

4. CONCLUSIONS

The application of SiNW FET devices for noninvasive time-course investigation of neuronal cell growth and differentiation using non-Faradaic EIS has been demonstrated. Using a precision LCR meter system, changes in the impedance of the cell−SiNW FET system caused by the attachment and differentiation of PC12 cells were observed. After modification with an APTMS SAM and PDL, our SiNW FET devices still demonstrated sensitivity to charged species in the environment by showing distinct responses for air, DI water, and growth medium. The APTMS/PDL-modified SiNW FET devices were able to monitor PC12 cell adhesion during cell growth by exhibiting changes in both impedance magnitude and impedance phase. The SiNW FET devices were also able to monitor morphological changes during PC12 neuronal differentiation on multi-SiNW FET devices by showing similar changes in the impedance parameters. Cell adhesion and neuronal differentiation could be distinguished using the time-course stabilization of the impedance parameters for the former and continued temporal changes of the parameters for the latter. The changes in impedance magnitude and impedance phase have been attributed to the high sensitivity of the SiNW devices to charged species and molecular layers in their immediate environment. In the case of monitoring the PC12 cells, changes in the impedance parameters were caused by the charged cell membrane and seal resistance at the cell/SiNW interface. The negatively charged cell membrane, in particular, varied the local carrier concentration in the SiNW channels depending on the extent of cell attachment onto or cellular coverage of the SiNW area.

The ability of the SiNW FET devices to monitor cell growth and differentiation, which lead to spreading on the sensor surface, can be also applied for investigating anomalous and nonelectrogenic cell behavior in toxin and drug screenings and for observing differentiation of stem cells. Single-SiNW FET devices can be used if individual cellular observations are desired, while multi-SiNW FET devices can be utilized if larger cells need to be probed or if the response of a group of cells needs to be determined. The measurement procedure is very straightforward and requires only a precision LCR meter. In combination with the amenability of SiNW FET devices to mass production and device integration, the cell-based biosensing technique proposed in this study can lead to the realization of low-cost sensing devices with potential applications in the fields of medicine, environmental science, and security.

■ ASSOCIATED CONTENT

Supporting Information

Measurement principle of non-Faradaic EIS, and additional experimental methods and data, including SEM images of single- and multi-SiNW FET devices, representation of full impedance spectra, time-course impedance measurement of blank hydrogel, video of confocal microscopy for the fluorescent observation of 3D cell-laden hydrogel, and optical microscopy images of PC12 cell growth. The Supporting Information is available free of charge on the ACS Publications website at DOI: 10.1021/acsami.5b01878.

■ AUTHOR INFORMATION

Corresponding Author

*Phone: +886-4-2284-0732 ext. 302. Fax: +886-4-2285-2422. E-mail: splin@dragon.nchu.edu.tw.

Author Contributions

§These authors contributed equally.

Notes

The authors declare no competing financial interest.

■ ACKNOWLEDGMENTS

Technical support for the fabrication of the SiNW FET devices was provided by National Nano Device Laboratories (Hsinchu, Taiwan). We would like to thank T. Y. Chi, C. C. Hsu, W. Y. Chang, S. Y. Huang, and J. Y. Ciou for their assistance in taking the SEM and confocal microscopic images. L.V. wishes to thank Dr. G. Yoshikawa for his words of advice and encouragement. This work was supported by the Ministry of Science and Technology of Taiwan under Contract Nos. NSC 100-2221-E-005-016-, NSC 101-2221-E-005-002-, NSC 101-2923-E-005-001-MY3, and NSC 102-2221-E-005-005-MY3. This work was supported in part by the Ministry of Education, Taiwan, under the ATU plan. L. Vinzons was a recipient of the Taiwan Scholarship Program.

DOI: 10.1021/acsami.5b01878
ACS Appl. Mater. Interfaces 2015, 7, 9866−9878

REFERENCES

(1) Fang, Y. Label-Free Cell-Based Assays with Optical Biosensors in Drug Discovery. *Assay Drug Dev. Technol.* **2006**, *4*, 583−595.
(2) Xi, B.; Yu, N.; Wang, X.; Xu, X.; Abassi, Y. The Application of Cell-Based Label-Free Technology in Drug Discovery. *Biotechnol. J.* **2008**, *3*, 484−495.
(3) Rodriguez-Mozaz, S.; Marco, M.-P.; de Alda, M.; Barceló, D. Biosensors for Environmental Applications: Future Development Trends. *Pure Appl. Chem.* **2004**, *76*, 723−752.
(4) Baeumner, A. J. Biosensors for Environmental Pollutants and Food Contaminants. *Anal. Bioanal. Chem.* **2003**, *377*, 434−445.
(5) Gu, M. B.; Mitchell, R. J.; Kim, B. C. In *Biomanufacturing;* Zhong, J.-J., Ed.; Springer: Berlin, Heidelberg, 2004; pp 269−305.
(6) Banerjee, P.; Bhunia, A. K. Cell-Based Biosensor for Rapid Screening of Pathogens and Toxins. *Biosens. Bioelectron.* **2010**, *26*, 99−106.
(7) Arora, P.; Sindhu, A.; Dilbaghi, N.; Chaudhury, A. Biosensors as Innovative Tools for the Detection of Food Borne Pathogens. *Biosens. Bioelectron.* **2011**, *28*, 1−12.
(8) Ding, L.; Du, D.; Zhang, X.; Ju, H. Trends in Cell-Based Electrochemical Biosensors. *Curr. Med. Chem.* **2008**, *15*, 3160−3170.
(9) Lin, S. P.; Kyriakides, T. R.; Chen, J. J. J. On-Line Observation of Cell Growth in a Three-Dimensional Matrix on Surface-Modified Microelectrode Arrays. *Biomaterials* **2009**, *30*, 3110−3117.
(10) Qureshi, A.; Gurbuz, Y.; Niazi, J. H. Probing Chemical Induced Cellular Stress by Non-Faradaic Electrochemical Impedance Spectroscopy Using an *Escherichia coli* Capacitive Biochip. *Analyst (Cambridge, U. K.)* **2011**, *136*, 2726−2734.
(11) Meissner, R.; Eker, B.; Kasi, H.; Bertsch, A.; Renaud, P. Distinguishing Drug-Induced Minor Morphological Changes from Major Cellular Damage *via* Label-Free Impedimetric Toxicity Screening. *Lab Chip* **2011**, *11*, 2352−2361.
(12) Katz, E.; Willner, I. Probing Biomolecular Interactions at Conductive and Semiconductive Surfaces by Impedance Spectroscopy: Routes to Impedimetric Immunosensors, DNA-Sensors, and Enzyme Biosensors. *Electroanalysis* **2003**, *15*, 913−947.
(13) Susloparova, A.; Koppenhofer, D.; Vu, X. T.; Weil, M.; Ingebrandt, S. Impedance Spectroscopy with Field-Effect Transistor Arrays for the Analysis of Anti-Cancer Drug Action on Individual Cells. *Biosens. Bioelectron.* **2013**, *40*, 50−56.
(14) Asphahani, F.; Zhang, M. Cellular Impedance Biosensors for Drug Screening and Toxin Detection. *Analyst (Cambridge, U. K.)* **2007**, *132*, 835−841.
(15) Sakmann, B.; Neher, E. Patch Clamp Techniques for Studying Ionic Channels in Excitable Membranes. *Annu. Rev. Physiol.* **1984**, *46*, 455−472.
(16) Stett, A.; Egert, U.; Guenther, E.; Hofmann, F.; Meyer, T.; Nisch, W.; Haemmerle, H. Biological Application of Microelectrode Arrays in Drug Discovery and Basic Research. *Anal. Bioanal. Chem.* **2003**, *377*, 486−495.
(17) Spira, M. E.; Hai, A. Multi-Electrode Array Technologies for Neuroscience and Cardiology. *Nat. Nanotechnol.* **2013**, *8*, 83−94.
(18) Tian, B.; Liu, J.; Dvir, T.; Jin, L.; Tsui, J. H.; Qing, Q.; Suo, Z.; Langer, R.; Kohane, D. S.; Lieber, C. M. Macroporous Nanowire Nanoelectronic Scaffolds for Synthetic Tissues. *Nat. Mater.* **2012**, *11*, 986−994.
(19) Soe, A. K.; Nahavandi, S.; Khoshmanesh, K. Neuroscience Goes on a Chip. *Biosens. Bioelectron.* **2012**, *35*, 1−13.
(20) Robinson, J. T.; Jorgolli, M.; Shalek, A. K.; Yoon, M.-H.; Gertner, R. S.; Park, H. Vertical Nanowire Electrode Arrays as a Scalable Platform for Intracellular Interfacing to Neuronal Circuits. *Nat. Nanotechnol.* **2012**, *7*, 180−184.
(21) Duan, X.; Gao, R.; Xie, P.; Cohen-Karni, T.; Qing, Q.; Choe, H. S.; Tian, B.; Jiang, X.; Lieber, C. M. Intracellular Recordings of Action Potentials by an Extracellular Nanoscale Field-Effect Transistor. *Nat. Nanotechnol.* **2012**, *7*, 174−179.
(22) Gao, R.; Strehle, S.; Tian, B.; Cohen-Karni, T.; Xie, P.; Duan, X.; Qing, Q.; Lieber, C. M. Outside Looking In: Nanotube Transistor Intracellular Sensors. *Nano Lett.* **2012**, *12*, 3329−3333.
(23) Cho, S.; Thielecke, H. Micro Hole-Based Cell Chip with Impedance Spectroscopy. *Biosens. Bioelectron.* **2007**, *22*, 1764−1768.
(24) Tian, B.; Cohen-Karni, T.; Qing, Q.; Duan, X.; Xie, P.; Lieber, C. M. Three-Dimensional, Flexible Nanoscale Field-Effect Transistors as Localized Bioprobes. *Science* **2010**, *329*, 830−834.
(25) Chen, K.-I.; Li, B.-R.; Chen, Y.-T. Silicon Nanowire Field-Effect Transistor-Based Biosensors for Biomedical Diagnosis and Cellular Recording Investigation. *Nano Today* **2011**, *6*, 131−154.
(26) Pui, T.-S.; Agarwal, A.; Ye, F.; Balasubramanian, N.; Chen, P. CMOS-Compatible Nanowire Sensor Arrays for Detection of Cellular Bioelectricity. *Small* **2009**, *5*, 208−212.
(27) Schäfer, S.; Eick, S.; Hofmann, B.; Dufaux, T.; Stockmann, R.; Wrobel, G.; Offenhäusser, A.; Ingebrandt, S. Time-Dependent Observation of Individual Cellular Binding Events to Field-Effect Transistors. *Biosens. Bioelectron.* **2009**, *24*, 1201−1208.
(28) Grieshaber, D.; MacKenzie, R.; Vörös, J.; Reimhult, E. Electrochemical Biosensors - Sensor Principles and Architectures. *Sensors* **2008**, *8*, 1400−1458.
(29) Li, B.-R.; Chen, C.-W.; Yang, W.-L.; Lin, T.-Y.; Pan, C.-Y.; Chen, Y.-T. Biomolecular Recognition with a Sensitivity-Enhanced Nanowire Transistor Biosensor. *Biosens. Bioelectron.* **2013**, *45*, 252−259.
(30) Zheng, G.; Patolsky, F.; Cui, Y.; Wang, W. U.; Lieber, C. M. Multiplexed Electrical Detection of Cancer Markers with Nanowire Sensor Arrays. *Nat. Biotechnol.* **2005**, *23*, 1294−1301.
(31) Cohen-Karni, T.; Timko, B. P.; Weiss, L. E.; Lieber, C. M. Flexible Electrical Recording from Cells Using Nanowire Transistor Arrays. *Proc. Natl. Acad. Sci. U.S.A.* **2009**, *106*, 7309−7313.
(32) Patolsky, F.; Timko, B. P.; Yu, G.; Fang, Y.; Greytak, A. B.; Zheng, G.; Lieber, C. M. Detection, Stimulation, and Inhibition of Neuronal Signals with High-Density Nanowire Transistor Arrays. *Science* **2006**, *313*, 1100−1104.
(33) Eschermann, J. F.; Stockmann, R.; Hueske, M.; Vu, X. T.; Ingebrandt, S.; Offenhäusser, A. Action Potentials of HL-1 Cells Recorded with Silicon Nanowire Transistors. *Appl. Phys. Lett.* **2009**, *95*, 083703−083703.
(34) Timko, B. P.; Cohen-Karni, T.; Yu, G.; Qing, Q.; Tian, B.; Lieber, C. M. Electrical Recording from Hearts with Flexible Nanowire Device Arrays. *Nano Lett.* **2009**, *9*, 914−918.
(35) Lin, S. P.; Chi, T. Y.; Lai, T. Y.; Liu, M. C. Investigation into the Effect of Varied Functional Biointerfaces on Silicon Nanowire MOSFETs. *Sensors* **2012**, *12*, 16867−16878.
(36) Gao, X. P.; Zheng, G.; Lieber, C. M. Subthreshold Regime has the Optimal Sensitivity for Nanowire FET Biosensors. *Nano Lett.* **2009**, *10*, 547−552.
(37) Peretz-Soroka, H.; Pevzner, A.; Davidi, G.; Naddaka, V.; Tirosh, R.; Flaxer, E.; Patolsky, F. Optically-Gated Self-Calibrating Nanosensors: Monitoring pH and Metabolic Activity of Living Cells. *Nano Lett.* **2013**, *13*, 3157−3168.
(38) Fohlerová, Z.; Skládal, P.; Turánek, J. Adhesion of Eukaryotic Cell Lines on the Gold Surface Modified with Extracellular Matrix Proteins Monitored by the Piezoelectric Sensor. *Biosens. Bioelectron.* **2007**, *22*, 1896−1901.
(39) Slaughter, G. E.; Hobson, R. An Impedimetric Biosensor Based on PC 12 Cells for the Monitoring of Exogenous Agents. *Biosens. Bioelectron.* **2009**, *24*, 1153−1158.
(40) Horváth, R.; Pedersen, H. C.; Skivesen, N.; Selmeczi, D.; Larsen, N. B. Optical Waveguide Sensor for On-Line Monitoring of Bacteria. *Opt. Lett.* **2003**, *28*, 1233−1235.
(41) Soussou, W. V.; Yoon, G. J.; Brinton, R. D.; Berger, T. W. Neuronal Network Morphology and Electrophysiology of Hippocampal Neurons Cultured on Surface-Treated Multielectrode Arrays. *IEEE Trans. Biomed. Eng.* **2007**, *54*, 1309−1320.
(42) Le Guillou-Buffello, D.; Bareille, R.; Gindre, M.; Sewing, A.; Laugier, P.; Amédée, J. Additive Effect of RGD Coating to Functionalized Titanium Surfaces on Human Osteoprogenitor Cell Adhesion and Spreading. *Tissue Eng., Part A* **2008**, *14*, 1445−1455.

DOI: 10.1021/acsami.5b01878
ACS Appl. Mater. Interfaces 2015, 7, 9866−9878

(43) McKeehan, W. L.; Ham, R. G. Stimulation of Clonal Growth of Normal Fibroblasts with Substrata Coated with Basic Polymers. *J. Cell Biol.* **1976**, *71*, 727−734.
(44) Lin, S. P.; Huang, S. Y.; Chen, S. F.; Vinzons, L. U.; Ciou, J. Y.; Wong, P. J. Investigation of the Interfacial Effects of Small Chemical-Modified TiO_2 Nanotubes on 3T3 Fibroblast Responses. *ACS Appl. Mater. Interfaces* **2014**, *6*, 12071−12082.
(45) Lin, S. P.; Liu, M. C.; Chi, T. Y.; Kang, Y. S. *Characterization of Functional Biointerface on Silicon Nanowire MOSFET. 33rd Annual International Conference of the IEEE EMBS, Boston* 2011, 4766−4769.
(46) Cui, Y.; Wei, Q.; Park, H.; Lieber, C. M. Nanowire Nanosensors for Highly Sensitive and Selective Detection of Biological and Chemical Species. *Science* **2001**, *293*, 1289−1292.
(47) Elisseeff, J.; Ruffner, M.; Kim, T.-G.; Williams, C. In *Culture of Cells for Tissue Engineering;* Vunjak-Novakovic, G., Freshney, R. I., Eds.; John Wiley & Sons, Inc.: Hoboken, NJ, 2006; Chapter 9, pp 213−238.
(48) Young, T.-H.; Hung, C.-H.; Huang, S.-W.; Hsieh, T.-S.; Hsu, J.-P. Determination of Surface Charge Properties of PC-12 Cells by Electrophoresis. *J. Colloid Interface Sci.* **2005**, *285*, 557−561.
(49) Vlodavsky, I.; Johnson, L.; Gospodarowicz, D. Appearance in Confluent Vascular Endothelial Cell Monolayers of a Specific Cell Surface Protein (CSP-60) not Detected in Actively Growing Endothelial Cells or in Cell Types Growing in Multiple Layers. *Proc. Natl. Acad. Sci. U.S.A.* **1979**, *76*, 2306−2310.
(50) Gruber, H. E.; Hanley, E. N. Human Disc Cells in Monolayer vs 3D Culture: Cell shape, Division and Matrix formation. *BMC Musculoskeletal Disord.* **2000**, *1*, 1−6.
(51) Vlodavsky, I.; Gospodarowicz, D. Respective Roles of Laminin and Fibronectin in Adhesion of Human Carcinoma and Sarcoma cells. *Nature* **1981**, *289*, 304−306.
(52) Mazia, D.; Schatten, G.; Sale, W. Adhesion of Cells to Surfaces Coated with Polylysine: Applications to Electron Microscopy. *J. Cell Biol.* **1975**, *66*, 198−200.
(53) Yu, L. M.; Wosnick, J. H.; Shoichet, M. S. Miniaturized System of Neurotrophin Patterning for Guided Regeneration. *J. Neurosci. Methods* **2008**, *171*, 253−263.
(54) Lelkes, P. I.; Unsworth, B. R.; Saporta, S.; Cameron, D. F.; Gallo, G. In *Culture of Cells for Tissue Engineering;* Vunjak-Novakovic, G., Freshney, R. I., Eds.; John Wiley & Sons, Inc.: Hoboken, NJ, 2006; Chapter 14, pp 375−415.

DOI: 10.1021/acsami.5b01878
ACS Appl. Mater. Interfaces 2015, 7, 9866−9878